Addressing and imaging high optical index dielectric ridges in the optical near field

Romain Quidant, Jean-Claude Weeber, and Alain Dereux
Laboratoire de Physique de l'Université de Bourgogne, Optique Submicronique, 9 Avenue A. Savary, F-21078 Dijon, France

David Peyrade
Laboratoire de Microstructures et Microélectronique (CNRS), 196 Avenue H. Ravera, F-92225 Bagneux, France

Gérard Colas des Francs and Christian Girard
Centre d'Elaboration des Matériaux et d'Etudes Structurales (CNRS), 29 Rue J. Marvig, F-31055 Toulouse, France

Yong Chen
Laboratoire de Microstructures et Microélectronique (CNRS), 196 Avenue H. Ravera, F-92225 Bagneux, France
(Received 8 June 2001; published 19 November 2001)

Experimental observation of light coupling between TiO_2 integrated waveguides of subwavelength cross section and pure three-dimensional evanescent light fields is reported. This near-field optical phenomenon is produced by controlling the location of the focusing of a laser beam totally reflected at the surface of the sample. The phenomenon is observed in direct space with a photon scanning tunneling microscope. Dielectric ridges several tens of micrometers long have been efficiently excited with this technique. Upon excitation, the extremities of the linear dielectric wires display intense light spots localized both inside and around the ridge. For ridge lengths up to 30 μm, the observed phenomenon has been reproduced numerically with a parallel implementation based on the three-dimensional Green dyadic method.

DOI: 10.1103/PhysRevE.64.066607 PACS number(s): 42.79.Gn, 07.79.Fc, 78.68.+m

I. INTRODUCTION

In modern optical communication technologies, transferring optical signals is often achieved by an optical waveguide connection [1]. When integrated in planar geometry, such devices can guide optical energy with low losses over several hundreds of micrometers. But when the cross section σ of the microfabricated waveguide is scaled down and reaches the diffraction limit ($\lambda \sim \sqrt{\sigma}$, where λ is the incident wavelength) its coupling with a standard excitation source is drastically hindered by two specific difficulties.

(i) Efficient coupling of light in such an optical waveguide requires perfect *alignment* of the wave vector of the incoming wave with the longitudinal axis of the guide.

(ii) Near the diffraction limit, the drastic decrease of available electromagnetic eigenmodes of the waveguide makes the use of standard optical couplers difficult. Direct focusing, prisms, and grating couplers are commonly used techniques. However, in the visible range, such couplers cannot be easily applied to structures with submicrometer transverse sections.

The present work explores different routes to overcome the difficulties arising from these two restrictive items. Solutions are proposed to achieve the efficient optical addressing of integrated waveguides featuring (a) transverse sizes ranging in the subwavelength domain (down to $\sigma \simeq 150\times 200$ nm^2); (b) modes confined laterally within a width of about half of the incident wavelength. The basic idea consists in the use of pure three-dimensional optical evanescent fields instead of the usual propagating laser beams. Such a state of the incident field can be produced by a three-dimensional (3D) Gaussian beam incident on the transparent substrate in such a way that it is totally reflected when there is no structure deposited on the surface of the said substrate. Recently, the pertinence of this coupling mode was checked in various configurations by extensive numerical simulations based on the Green dyadic technique [2]: the reduction of the transverse section of a waveguide has to be balanced by increasing the contrast of the dielectric functions between the constitutive material and the surrounding media, namely, the air and the glass substrate in our case [3]. Actually, a dielectric function of about 5.0 allows us to achieve our purpose.

II. MICROFABRICATION OF SUBWAVELENGTH OPTICAL WAVEGUIDES

The sample used in this work was obtained by standard electron-beam lithography and reactive ion etching techniques (see Fig. 1). First, a 150 nm thick TiO_2 layer was coated on a glass substrate (residual roughness 1 nm) by ion assisted deposition. This deposition technique enables one to obtain a TiO_2 layer with a residual roughness of 3 nm, which was found to be sufficient for significant optical measurements. In the second step, electron-beam patterning was performed by a JEOL 5D2U vector scan generator operating at 50 keV energy on a single layer of polymethylmethacrylate (PMMA) resist (950×10^3 molecular weight and 150 nm thickness). The *e*-beam current used in this work is 1 nA, which permits us to have a beam spot size of 30 nm. After development of the PMMA film, a nickel coating is evaporated onto the surface and lifted off by dissolution of the PMMA. Reactive ion etching is then performed in a Nextral NE110 system equipped with parallel plate electrodes and a silicon cathode. The etching process uses a $SF_6(0.5)/CHF_3(0.5)$ equal flow rate gas mixture at a pres-

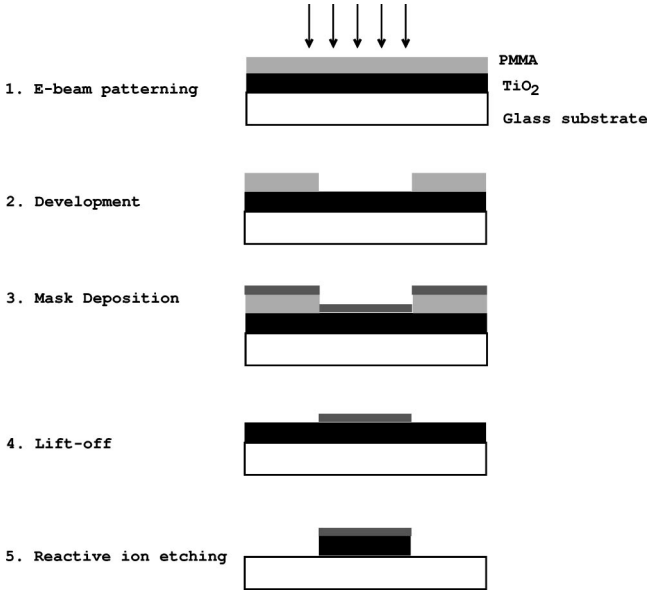

FIG. 1. Schematic description of the TiO_2 waveguide fabrication process.

sure of 10 mT and a rf power of 20 W, which produces a self-induced bias voltage of -190 V. The etching rate is typically 50 nm/min and the reactive ion etching parameters are optimized for steeper sidewalls. Finally, the remaining Ni mask is removed in nitrite acid solution (not shown in Fig. 1). The resulting sample consists of a planar glass surface supporting a large number of subwavelength optical waveguides (SOW's) that all display the same geometrical parameters (40 μm long, 200 nm wide, and 150 nm high). Figure 2 presents a scanning electron microscope picture of a TiO_2 waveguide after etching and deposition of a thin gold layer (10 nm) to avoid charge effects. The whole dielectric ridge is shown in Fig. 2(a) and a magnification of its extremity is displayed in Fig. 2(b). The roughness revealed by this picture originates from the metal deposition. The spacing ($\simeq 20$ μm) between each SOW was chosen sufficiently large to prevent any coupling between them.

III. NEAR-FIELD OPTICAL ADDRESSING OF A SINGLE SOW

This sample was then mounted on the prism of a photon scanning tunneling microscope (PSTM) [4] (see Fig. 3). In a PSTM, a pointed tip is piezoelectrically driven to scan close to the sample surface so as to act as a local probe of the optical field in the near-field zone [4–10]]. The sharply elongated tips were obtained by pulling an optical fiber which was subsequently coated with 7 nm of Cr (no resulting aperture). The PSTM was scanning at constant height. In this mode of operation, the signal detected by a PSTM is well known to be related to the spatial distribution of the intensity of the optical electric field in the near-field zone (I_{nf}) [11,12]. This configuration of a scanning near-field optical microscope has proved to be an efficient technique to characterize, in direct space and with subwavelength resolution, the optical properties of waveguides [13–17] or nanostructures integrated in coplanar geometry [18–20]. Specifically, the PSTM turned out to be well suited to map the propagation of light at the submicrometer scale [12].

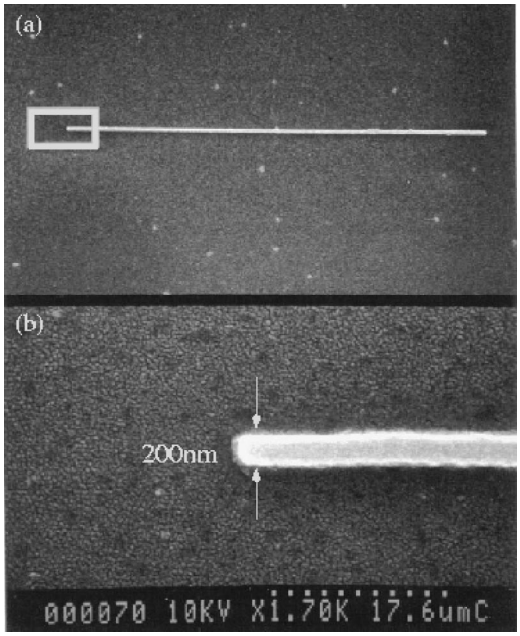

FIG. 2. Scanning electron microscopy picture of a TiO_2 waveguide after the deposition of a thin gold layer (10 nm thick). The top image (a) shows the whole waveguide (40 μm long, 200 nm wide, and 150 nm high) and the bottom one (b) presents a magnification of the waveguide extremity inside the rectangle overlying image (a).

For our purpose, the specific feature of the PSTM setup is the incident field: instead of the usual extended plane wave, we used a focused Gaussian beam which is totally reflected at the substrate interface. Some years ago a similar configuration was introduced by Dawson *et al.* to trigger localized propagations of plasmon polaritons [9,21]. In the present work, this local illumination is produced by a He-Ne laser (wavelength in vacuum 633 nm) injected in a lensed single mode fiber. The extremity of the fiber is oriented in such a way that the beam can be focused at the interface between the dielectric ridge and the glass substrate. We considered only the case of a transverse magnetic (TM) polarized inci-

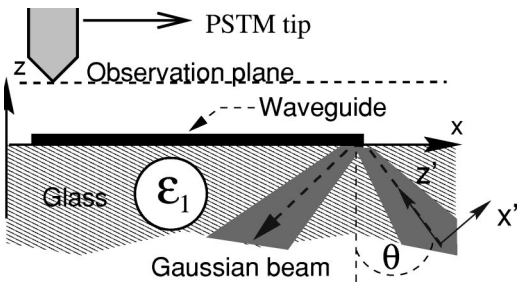

FIG. 3. Geometry of the device. An isolated SOW lying on the surface of a glass substrate (dielectric function ε_1) is illuminated by a Gaussian beam reflected at the interface between the substrate and the upper medium (air). The near-field optical detection is achieved by scanning with the tip of a PSTM.

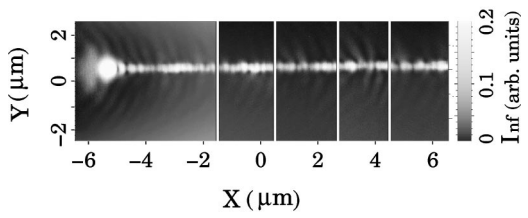

FIG. 4. Assembling of five 5 μm$\times$5 μm PSTM images recorded above the last quarter of the SOW. The left image, where a spot shows up, was recorded above the ''exit'' end of the SOW.

dent beam where the effect is expected to be more pronounced [2].

The Gaussian beam is now focused at the right extremity of the SOW in such a way that the components of the incident wave vector parallel to the surface of the substrate are aligned along the longitudinal axis of the SOW. The tip is scanned at a constant height above the sample surface while monitoring the light intensity level. Successive images were recorded while approaching the tip closer and closer to the surface of the sample.

In order to improve the visualization of the light localization phenomenon inside the SOW, one has to get rid of the problem of parallelism between the tip trajectory and the surface of the substrate. This is possible by obtaining five successive PSTM images of size 5×5 μm^2 recorded above the last quarter of the SOW by keeping the distance between the tip and the top of the SOW between 10 and 50 nm. The corresponding results are gathered in Fig. 4. In order to clearly visualize the lower intensities detected over the ridge, the scale of the left image was truncated to match the intensity range of the other four images. This left image details the precise shape of the light spot that tails off the excited SOW. It is intense and well localized with an effective area of about 0.4 μm^2. In spite of the subwavelength transverse size of the SOW, the mode remains well confined inside the structure. The full width at half maximum of the spatial distribution of the intensity of the mode along the transverse (y) direction is found to be around 300 nm. A clear identification of this mode is possible only by using a PSTM.

IV. MODELING THE LIGHT TRANSFER PROCESS

A. The zeroth order solution $\mathbf{E_0}(\mathbf{r},\omega)$

A proper simulation of the experimental observations reported in the previous section needs to describe the physical interaction between the optical eigenmodes supported by the TiO_2 ridge and the *evanescent light spot*. To achieve this purpose, we consider the geometry depicted in Fig. 5. First we start from the known solutions associated with a simple planar optical junction excited beyond the critical angle for total reflection by a focused laser beam [see Fig. 5(a)]. The spatial distribution of this *evanescent light spot* can be described from previous modeling [22,23,2]. At a given vector point $\mathbf{r}=(x,y,z)$ above the reference surface we can write

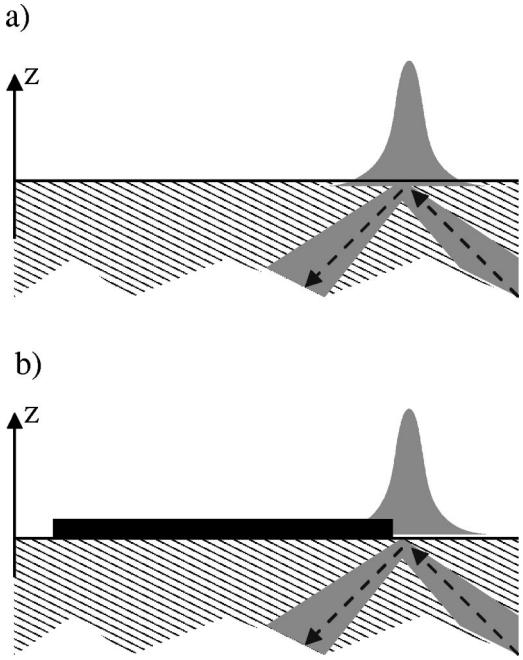

FIG. 5. Schematic description of the model used in our simulations. (a) The reference system for which the solution is known; (b) the final system for which the solution is to be determined.

$$\begin{aligned}\mathbf{E}_0(\mathbf{r},\omega)=&\int_{-\sqrt{\varepsilon_1}(\omega/c)\cos\theta}^{\sqrt{\varepsilon_1}(\omega/c)\cos\theta} d\alpha\\ &\times\int_{-\sqrt{\varepsilon_1(\omega^2/c^2)\cos^2\theta-\alpha^2}}^{\sqrt{\varepsilon_1(\omega^2/c^2)\cos\theta-a^2}}\\ &\times d\beta\,\vec{\zeta}^{(\mathrm{T})}\exp[-w_0^2(\alpha^2+\beta^2)/4]\\ &\times\exp[ik_x(x-x_0)+ik_y(y-y_0)+ik_z^{(3)}(z-z_0)],\end{aligned}\tag{1}$$

where (x_0,y_0,z_0) represents the position of the focal point in the initial, unrotated system of coordinates (x,y,z). As usual, $k_z^{(3)}$ is defined by $k_z^{(3)}(\alpha,\beta)=(\omega^2/c^2-k_x^2-k_y^2)^{1/2}$. The tangential components of $\vec{\zeta}^{(\mathrm{T})}$ obey the following equation:

$$\begin{pmatrix}\zeta_x^{(\mathrm{T})}\\ \zeta_y^{(\mathrm{T})}\end{pmatrix}=\mathbf{A}\begin{pmatrix}\zeta_{\mathrm{inc},x}\\ \zeta_{\mathrm{inc},y}\end{pmatrix},\tag{2}$$

where $\mathbf{A}$ is a (2×2) matrix given by

$$\mathbf{A}=\begin{pmatrix}(\tau_\parallel-\tau_\perp)\cos^2\delta+\tau_\perp & (\tau_\parallel-\tau_\perp)\cos\delta\sin\delta\\ (\tau_\parallel-\tau_\perp)\cos\delta\sin\delta & (\tau_\parallel-\tau_\perp)\sin^2\delta+\tau_\perp\end{pmatrix},\tag{3}$$

in which $\tau_\parallel$ and $\tau_\perp$ represent the Fresnel coefficients of the bare surface, and δ labels the angle between the x axis of the fixed system of coordinates and the direction of $\vec{k}_\parallel(\alpha,\beta)=k_x(\alpha,\beta)\vec{x}+k_y(\alpha,\beta)\vec{y}$. Finally, the third component $\zeta_z^{(\mathrm{T})}$ is merely deduced from the tangential components by using the relation $\vec{\nabla}\cdot\vec{\zeta}^{(\mathrm{T})}=0$.

B. Self-consistent field inside the ridge guide

To properly describe the complex optical coupling between the microfabricated SOW and the focused evanescent field $\mathbf{E}_0(\mathbf{r},\omega)$, we first discretize the entire volume $\mathcal{V}$ of the SOW into small elementary cells of volume v_i. At each position $\mathbf{R}_i$ of the discretization grid, the local field is then computed from the relation

$$\mathbf{E}(\mathbf{R}_i,\omega)=\sum_j \mathcal{K}(\mathbf{R}_i,\mathbf{R}_j,\omega)\cdot\mathbf{E}_0(\mathbf{R}_j,\omega), \tag{4}$$

where $\mathcal{K}$ labels the generalized field propagator of the entire system (waveguide plus bare surface) [24]. Within the $\{\mathbf{R}_i;\mathbf{R}_j\}$ representation, it is given by

$$\mathcal{K}(\mathbf{R}_i,\mathbf{R}_j,\omega)=\delta_{i,j}+v_j\mathcal{S}(\mathbf{R}_i,\mathbf{R}_j,\omega)\cdot\chi(\mathbf{R}_j,\omega), \tag{5}$$

where χ represents the electric susceptibility of the guide's material and $\mathcal{S}$ is the field susceptibility of the entire system. This last quantity is usually computed by solving Dyson's equation:

$$\mathcal{S}(\mathbf{R}_i,\mathbf{R}_j,\omega)=\mathbf{S}_0(\mathbf{R}_i,\mathbf{R}_j,\omega)+\sum_k v_k \times\mathbf{S}_0(\mathbf{R}_i,\mathbf{R}_k,\omega)\cdot\chi(\mathbf{R}_k,\omega)\cdot\mathcal{S}(\mathbf{R}_k,\mathbf{R}_j,\omega), \tag{6}$$

in which the dyadic tensor $\mathbf{S}_0$ describes the electric response of the bare surface [25]. Analytical expressions for this tensor can be found in the literature (see, for example, Ref. [25]). Moreover, efficient numerical evaluation methods of these tensors can be found in Refs. [26,27]. Note that the implicit character of this last equation ensures the self-consistency of the solution and thereby the self-consistency of the field calculation inside the dielectric ridge.

C. Numerical simulation of the electric field maps

The local detection of the optical signal relies on the use of nanometer-sized probes. As already mentioned above, pointed dielectric detectors usually detect the square modulus of the optical near field generated by the object under study. The continuous description of this field vector can be derived from a revised version of the Huygens-Fresnel principle in which the elementary sources must be excited by the self-consistent fields $\mathbf{E}(\mathbf{R}_j,\omega)$ instead of the incident field:

$$\mathbf{E}(\mathbf{r},\omega)=\mathbf{E}_0(\mathbf{r},\omega)+\sum_i v_i\mathbf{S}_0(\mathbf{r},\mathbf{R}_i,\omega)\cdot\chi(\mathbf{R}_i,\omega)\cdot\mathbf{E}(\mathbf{R}_i,\omega). \tag{7}$$

In the numerical work to be discussed in this section, the SOW has the same section as that of the sample studied above but, in order to keep a reasonable calculation time, its length was reduced to 30 μm. The modeling assumed a perfect rod of TiO_2 (optical index 2.3) supported by a half space filled with glass (optical index 1.46).

In Fig. 6, the SOW is locally illuminated by a monochromatic 3D beam whose angular frequency ω defines a wavelength in vacuum $\lambda=2\pi c/\omega=633$ nm and a beam waist $w_0=2\lambda$. In this example, the intensity is normalized with respect to the intensity of the incident field lying under the surface. Revealing the excitation of a guided mode inside the SOW, an electric field intensity of the same order of magnitude as the reference intensity can be observed around the complete dielectric structure. As expected intuitively, the efficiency of this coupling is optimized when the Gaussian

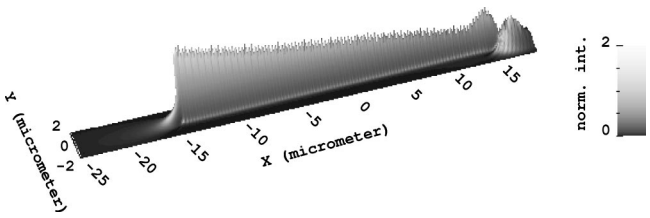

FIG. 6. Three-dimensional view of the electric near-field intensity computed 50 nm over a 30.0 μm long homogeneous SOW locally excited by a Gaussian beam.

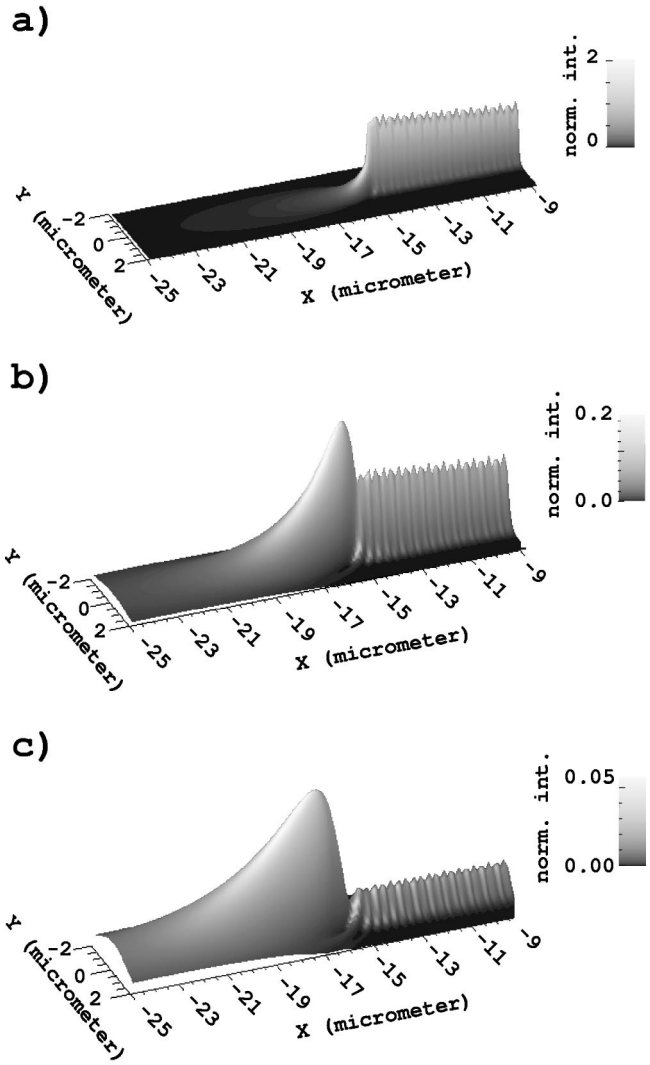

FIG. 7. Sequence of three images showing the evolution of the field at the SOW exit when the observation distance is increased. (a) $Z_{ob}=200$ nm, (b) $Z_{ob}=500$ nm, and (c) $Z_{ob}=800$ nm.

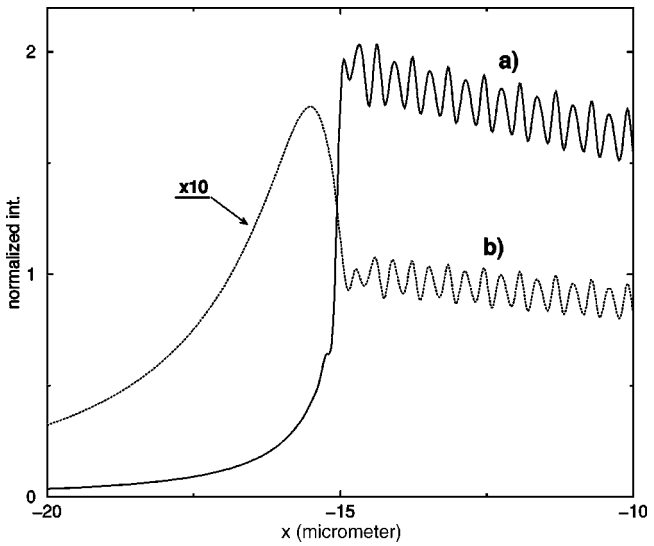

FIG. 8. Variation of the optical electric near-field intensity along the longitudinal axis of the SOW. (a) The calculation was made at 200 nm from the surface; (b) same as (a) but for 500 nm.

beam is aligned with the axis of the waveguide. We can interpret this phenomenon as a consequence of the Goos-Hänschen shift that usually occurs in this configuration.

We notice a striking analogy between Fig. 7 and the experimental map given in Fig. 4. In this case, the field intensity is calculated, over the end of the wire, for different observation distances. Increase of the calculation height partially restores the proportions of the detected intensity at the end of the SOW even if the exit spot appears much more extended than in the experiments. This tendency shows that some of the electric field components at the output are radiative. Of course, this calculation configuration does not match the conditions of the experiments where the probe is scanned only several tenths of nanometers above the structure. Nevertheless, considering a higher calculation plane is a way to include effects arising from the finite size of the detector.

Finally, it may be seen that a cross cut along the longitudinal (x) axis of the SOW in the calculated image exhibits a standing wave pattern which does not show up so sharply in the experiment. This standing wave pattern (see Fig. 8) arises due to the interferences of the incoming light with the light reflected back at the end of the SOW. The topography of the sample, as recorded by an atomic force microscope (not shown for the sake of brevity), reveals a significant roughness ($\simeq 15$ nm) at the surface of the TiO_2 wires. The resulting random scattering probably produces the observed fuzzier standing wave pattern.

V. CONCLUSION

The experiments described in this paper clearly demonstrate that dielectric ridges, featuring both transverse sizes in the subwavelength range, can guide light at visible frequencies. The guiding process relies on the lowest frequency mode sustained by the device. On the basis of the Goos-Hänschen effect, such a mode can be excited locally at the ''entry'' end of the SOW by focusing a totally reflected Gaussian beam. We have thus shown that this nonstandard coupling technique is efficient to excite narrow waveguides in coplanar geometry. In agreement with theoretical predictions, PSTM images have revealed, in direct space, the excitation of the SOW lowest mode over several tens of micrometers. This mode is confined laterally within a width of about half of the incident wavelength. Finally, the well-localized light spots observed at the SOW ''exit'' could be used to address optically nanoscopic objects deposited on a surface. In particular, among the various applications of the phenomenon demonstrated above, the optical addressing of a single molecule in planar geometry can complete the local probe based methods described in the literature [28]. Further development of this concept could lead to the realization of subwavelength optical devices that could be integrated in planar geometry.

ACKNOWLEDGMENTS

This work was funded by the Regional Council of Burgundy and by the French Ministry for Education and Research through the program ''Nanostructures et Fonctionnalités.'' In addition, we have benefited from the computing facilities provided by the massively parallel center CALMIP of Toulouse.

[1] W.K. Burns and A.F. Milton, in *Guided-Wave Optoelectronics*, edited by T. Tamir (Springer, Berlin, 1988).
[2] J. Weeber *et al.*, Phys. Rev. E **62**, 7381 (2000).
[3] C. Girard, A. Dereux, and C. Joachim, Europhys. Lett. **44**, 686 (1998).
[4] R.C. Reddick, R.J. Warmack, and T.L. Ferrell, Phys. Rev. B **39**, 767 (1989).
[5] D. Courjon, K. Sarayedine, and M. Spajer, Opt. Commun. **71**, 23 (1989).
[6] J.M. Vigoureux, C. Girard, and D. Courjon, Opt. Lett. **14**, 1039 (1989).
[7] S. Jiang, N. Tomita, H. Ohsawa, and M. Ohtsu, Jpn. J. Appl. Phys., Part 1 **30**, 2107 (1991).
[8] N.F. van Hulst, F.B. Segerink, F. Achten, and B. Bolger, Ultramicroscopy **42**, 416 (1992).
[9] P. Dawson, F. de Fornel, and J.P. Goudonnet, Phys. Rev. Lett. **72**, 2927 (1994).
[10] T. Saiki, M. Ohtsu, K. Jang, and W. Jhe, Opt. Lett. **21**, 674 (1996).
[11] J.C. Weeber *et al.*, Phys. Rev. Lett. **77**, 5332 (1996).
[12] J.R. Krenn *et al.*, Phys. Rev. Lett. **82**, 2590 (1999).
[13] N. Van Hulst, M. Moers, and E. Borgonjen, in *Photons and Local Probes*, Vol. 300 of *NATO Advanced Study Institute, Series E: Applied Sciences*, edited by O. Marti and R. Möller (Kluwer, Dordrecht, 1995), pp. 165–180.
[14] E. Bourillot *et al.*, Phys. Rev. B **51**, 11 225 (1995).

[15] M.L.M. Balistreri *et al.*, Opt. Lett. **25**, 637 (2000).
[16] M.L.M. Balistreri, J.P. Korterik, L. Kuipers, and N.F. van Hulst, Phys. Rev. Lett. **85**, 294 (2000).
[17] E. Flück *et al.*, J. Microsc. **202**, 104 (2001).
[18] D. Mullin *et al.*, J. Appl. Phys. **87**, 534 (2000).
[19] S. Davy, D. Barchiesi, M. Spajer, and D. Courjon, Eur. Phys. J.: Appl. Phys. **5**, 277 (1999).
[20] D. Mullin *et al.*, J. Microsc. **202**, 110 (2004).
[21] P. Dawson, B.A.F. Puygranier, and J.P. Goudonnet, Phys. Rev. B **63**, 205410 (2001).
[22] F.I. Baida, D. Van Labeke, and J.M. Vigoureux, Ultramicroscopy **71**, 351 (1998).
[23] F.I. Baida, D. Van Labeke, and J.M. Vigoureux, Phys. Rev. B **60**, 7812 (1999).
[24] O.J.F. Martin, C. Girard, and A. Dereux, Phys. Rev. Lett. **74**, 526 (1995).
[25] C. Girard, A. Dereux, O.J.F. Martin, and M. Devel, Phys. Rev. B **52**, 2889 (1995).
[26] P. Gay-Balmaz and O.J.F. Martin, Opt. Commun. **184**, 37 (2000).
[27] M. Paulus, P. Gay-Balmaz, and O.J.F. Martin, Phys. Rev. E **62**, 5797 (2000).
[28] E. Betzig and R.J. Chichester, Science **262**, 1422 (1993).